

# Momentum distribution of the uniform electron gas: improved parametrization and exact limits of the cumulant expansion

Paola Gori-Giorgi<sup>1</sup> and Paul Ziesche<sup>2</sup>

<sup>1</sup> *INFM Center for Statistical Mechanics and Complexity,  
and Dipartimento di Fisica, Università di Roma “La Sapienza”,  
Piazzale A. Moro 2, I-00185 Rome, Italy*

<sup>2</sup> *Max-Planck-Institut für Physik komplexer Systeme  
Nöthnitzer Str. 38, D-01187 Dresden, Germany*

(Dated: December 2, 2024)

## Abstract

The momentum distribution of the unpolarized uniform electron gas in its Fermi-liquid regime,  $n(k, r_s)$ , with the momenta  $k$  measured in units of the Fermi wave number  $k_F$  and with the density parameter  $r_s$ , is constructed with the help of the convex Kulik function  $G(x)$ . It is assumed that  $n(0, r_s)$ ,  $n(1^\pm, r_s)$ , the on-top pair density  $g(0, r_s)$  and the kinetic energy  $t(r_s)$  are known (respectively, from effective-potential calculations, from the solution of the Overhauser model, and from Quantum Monte Carlo calculations via the virial theorem). Information from the high- and the low-density limit, corresponding to the random-phase approximation and to the Wigner crystal limit, is used. The result is an accurate parametrization of  $n(k, r_s)$ , which fulfills most of the known exact constraints. It is in agreement with the effective-potential calculation of Takada and Yasuhara [1991 *Phys. Rev. B* **44** 7879], is compatible with Quantum Monte Carlo data, and is valid in the density range  $r_s \lesssim 12$ . The corresponding cumulant expansions of the pair density and of the static structure factor are discussed, and some exact limits are derived.

PACS numbers: 71.10.Ca, 05.30.Fk

## I. INTRODUCTION

In solid state theory [1] and quantum chemistry [2], the phenomenon of electron correlation and some of its details are hidden in the reduced densities and reduced density matrices [3, 4, 5, 6] and their cumulants [7, 8]. For the ground state of the uniform electron gas (jellium) of density  $\rho = 3/(4\pi r_s^3)$  (in a.u.), these quantities are the pair density  $g(x, r_s)$  and the momentum distribution  $n(k, r_s)$ , where  $k$  is measured in units of  $k_F$  and  $x$  is the scaled interelectronic distance,  $x = k_F r_{12}$ . They are contained in the cumulant 2-matrix  $\chi(1|1', 2|2')$  [7, 8], which thus rises to be a key quantity. Recently, the pair density  $g(x, r_s)$  has been diagonalized in terms of Overhauser geminals [9, 10, 11], and there have been attempts to calculate the jellium  $\chi(1|1', 2|2')$  [12, 13].

In Ref. [14], the idea of using the Kulik function  $G(x)$  for a proper parametrization of  $n(k, r_s)$  for all  $k$ , is sketched. The function  $G(x)$  appeared in Kulik's [15] random-phase approximation (RPA) analysis of  $n(k, r_s)$  near the Fermi edge ( $|1-k| \ll 1$ ).  $G(x)$  is convex and behaves as  $c_0 + c_1 x \ln x$  for small  $x$  (see Appendix A and Fig. 1), which corresponds to the correct behavior of  $n(k, r_s)$  near the Fermi surface (both in the Fermi liquid regime, with a non-vanishing Fermi gap at  $k = 1$ , as well as in the non-Fermi-liquid regime, with a continuous  $n(k, r_s)$  vs.  $k$ ). So, supposing that the value at the centre,  $n(0, r_s)$ , and the values at the Fermi edge,  $n(1^-, r_s)$  and  $n(1^+, r_s)$ , are known, it should be possible to represent  $n(k, r_s)$  (which is a concave function of  $k$  for  $k < 1$  and a convex function of  $k$  for  $k > 1$ ) in terms of  $G(x)$ , with suitable prefactors and with suitable scaling (squeezing and stretching) of its argument. In this way,  $n(k, r_s)$  becomes a functional of  $n_0(r_s) = n(0, r_s)$  and of  $n_{\pm}(r_s) = n(1^{\pm}, r_s)$ , and can be designed to yield the proper normalization and the correct kinetic energy  $t(r_s)$ , which follows from the total energy  $\epsilon(r_s) = t(r_s) + v(r_s)$  via the virial theorem [16]. In addition to these two quantitative sum rules, there are infinite qualitative conditions requiring  $n(k, r_s)$  and all the related functions to be as smooth as possible. In Ref. [14], the input data from Takada and Yasuhara (TY) [17, 18] for  $n_0(r_s)$ ,  $n_{\pm}(r_s)$  and  $t(r_s)$  at  $r_s = 1, \dots, 5$  have been used, together with the on-top pair density  $g_0(r_s) = g(0, r_s)$  [which determines the large- $k$  behavior of  $n(k, r_s)$ ] from Ref. [10]. The result was a field  $n(k, r_s)$  for  $r_s \in [1, 6]$  which was correctly concave for  $k < 1$ , convex for  $k > 1$ , and with a Fermi gap  $z_F(r_s) = n_-(r_s) - n_+(r_s)$  at  $k = 1$  decreasing with growing  $r_s$ . The attempt to extend this same procedure for  $r_s \in [6, 10]$  failed:  $n(k < 1, r_s)$  was no longer concave for

$r_s \gtrsim 6$ .

Here, an improved version of the parametrization of  $n(k, r_s)$  in terms of the Kulik function  $G(x)$  is presented. Our parametrized momentum distribution is in good agreement with the TY values [17, 18], and is valid in the range of densities  $r_s \lesssim 12$ . Previous parametrizations of  $n(k, r_s)$  [19, 20, 21, 22] used the Quantum Monte Carlo (QMC) data of Ref. [19] as an input. However, QMC data are presently only available for  $0.4 \lesssim k \lesssim 0.9$  and  $1.1 \lesssim k \lesssim 1.5$ , thus not providing information about  $n(k, r_s)$  near the centre,  $k = 0$ , and at the Fermi edge,  $k = 1$ . In these last regions, in fact, different parametrizations of the same QMC data can be rather different from each other [19, 20, 21]. Our construction of  $n(k, r_s)$  uses information from the effective-potential calculation of Takada and Yasuhara [17, 18], from the high- and low-density limits of  $n(k, r_s)$ , corresponding to RPA and the Wigner crystal (WC) limit, and from accurate parametrizations of  $t(r_s)$  [23] and of  $g_0(r_s)$  [10]. In the regions where QMC data are available, our  $n(k, r_s)$  seems to be compatible with them. Also, with respect to previous works [19, 20, 21, 22], the functional form used here satisfies more exact limits. In particular, the logarithmic behavior at the Fermi edge is taken into account for the first time [24]. Notice that it causes the logarithmic divergence of  $t(r_s \rightarrow 0)$  [25].

Using our  $n(k, r_s)$ , the moments  $\langle k^\nu \rangle$ , the correlation entropy, and the one-body reduced density matrix  $f(x, r_s)$  are evaluated. The latter appears in the cumulant partitioning of the pair density  $g(x, r_s)$ . The static structure factor  $S(k, r_s)$ , related to the pair density via Fourier transform, the particle-number fluctuation in fragments  $\Delta N_\Omega(r_s)$ , and the potential energy  $v(r_s)$  are discussed in terms of their cumulant partitionings, and some exact limits are derived. Finally, by means of accurate models for the pair density [26, 27, 28, 29], the cumulant part of  $g(x, r_s)$  is extracted.

The paper is organized as follows. In Sec. II, the known sum rules and limiting cases for  $n(k, r_s)$  are reported, and they are used in Sec. III to build up our parametrization of the momentum distribution via the Kulik function. Sec. IV is devoted to the calculation and discussion of different measures of the correlation strength, of the one-matrix, and of the cumulant expansion of the pair-density. In Sec. V, we study the cumulant partitioning of the static structure factor, of the density fluctuations and of the potential energy. Conclusions and future developments are reported in the last Sec. VI.

## II. SUM RULES AND LIMITING CASES

How is  $n(k, r_s)$  defined? Starting from the many-body wave function  $\Psi(1, \dots, N)$ , the one-body reduced density matrix (1-matrix for short) results from the  $N - 1$  contraction

$$\gamma(1|1') = \int \frac{d2\dots dN}{(N-1)!} \Psi(1, 2, \dots, N) \Psi^*(1', 2, \dots, N), \quad \int \frac{d1\dots dN}{N!} |\Psi(1, \dots, N)|^2 = 1, \quad (1)$$

with the notation  $1 \equiv (\underline{r}_1, \sigma_1)$ . For the uniform electron gas,  $\gamma(1|1') = \rho \delta_{\sigma_1 \sigma_1'} f(k_F |\underline{r}_1 - \underline{r}_1'|, r_s)$  defines the dimensionless 1-matrix  $f(x, r_s)$ . Then its Fourier transform is the momentum distribution

$$n(k, r_s) = \frac{\alpha^3}{2} \int_0^\infty dx^3 \frac{\sin kx}{kx} f(x, r_s), \quad (2)$$

where  $dx^3 = 3/4\pi d^3x = 3x^2 dx$ , and  $\alpha = (4/9\pi)^{1/3}$ .  $n(k, r_s)$  can be calculated using perturbation theory, directly with Green's functions [15], see Figs. 1a and 1b of Ref. [12], or via the Hellmann-Feynman theorem as the energy-derivative  $n(k, r_s) = \delta E / \delta \varepsilon_k$ , supposed  $E$  is (perturbatively) known as a functional of  $\varepsilon_k = \hbar k^2 / 2m$  and  $v_q = 4\pi e^2 / q^2$  [30]. Perturbative methods only work for high-denisties,  $r_s \ll 1$ . At metallic and lower densities, other techniques must be used, namely, the effective-potential method [17], which combines perturbation theory (Green's functions) with the Fermi-hypernetted chain approach, and the QMC simulations [19, 31]. A more complete list of references concerning calculations and parametrizations can be found in Ref. [14].

$n(k, r_s)$  has to satisfy the condition  $0 < n(k, r_s) < 1$  (which guarantees the  $N$ -representability of the 1-matrix), and the sum rules ( $k$  in units of  $k_F$ , and energies in ryd)

$$\int_0^\infty dk^3 n(k, r_s) = 1, \quad (3)$$

$$\frac{1}{(\alpha r_s)^2} \int_0^\infty dk^3 n(k, r_s) k^2 = t(r_s), \quad (4)$$

where  $t(r_s)$  can be written as the sum of the kinetic energy of the free Fermi gas,  $3/5 (\alpha r_s)^{-2}$ , and of the kinetic energy of correlation,  $t_{\text{corr}}(r_s)$ . For  $r_s \ll 1$ ,  $t_{\text{corr}}(r_s)$  is known from RPA and from the lowest-order exchange diagram beyond it [33, 34, 35]; for a summary see Eq. (3.25) and Figs. 1a and 1b of Ref. [12]. At larger  $r_s$ ,  $t_{\text{corr}}(r_s)$  can be obtained via the virial theorem [16] from parametrized QMC correlation energies [23].

The large- $k$  behavior of  $n(k, r_s)$  is determined by the kinks in the many-body wavefunction which occur whenever two electrons are at contact or “on-top” (coalescing cusp

properties) [36, 37],

$$n(k \rightarrow \infty, r_s) = \frac{8}{9\pi^2} (\alpha r_s)^2 \frac{g_0(r_s)}{k^8} + O\left(\frac{1}{k^{10}}\right), \quad (5)$$

where  $g_0(r_s) = g(0, r_s)$  is the on-top value of the pair-correlation function. In the  $r_s \rightarrow 0$  limit,  $g_0(r_s)$  can be obtained from perturbation theory [38, 39], and at larger  $r_s$  it has been calculated by solving an effective two-body Schrödinger equation [10]. Notice [40].

In a normal Fermi liquid [41], the momentum distribution has a discontinuity and infinite slopes [42] at the Fermi edge,  $k = 1$ ,

$$n(k \rightarrow 1^-, r_s) = n_-(r_s) - A(r_s)(1 - k) \ln(1 - k) + O(1 - k), \quad (6)$$

$$n(k \rightarrow 1^+, r_s) = n_+(r_s) + A(r_s)(k - 1) \ln(k - 1) + O(k - 1). \quad (7)$$

In the following,  $A(r_s)$  is referred to as the Fermi edge coefficient. In the small- $r_s$  limit,  $n_{\pm}(r_s)$  and  $A(r_s)$  are known from RPA (see Appendix A). In the low-density or WC limit, the Fermi gap disappears [ $n_-(r_s) \rightarrow n_+(r_s)$ ], the infinite slopes at the Fermi edge may also vanish [ $A(r_s) \rightarrow 0$ ], see Appendix C.

Near the centre,  $k \rightarrow 0$ ,  $n(k, r_s)$  should behave quadratically [20, 21, 22, 31],

$$n(k \rightarrow 0, r_s) = n_0(r_s) + B(r_s)k^2 + O(k^4). \quad (8)$$

A simple argument in favour of Eq. (8) is that it holds both in the high- and in the low-density limit (see Appendix A and B).

When  $r_s \rightarrow 0$ , exact results for  $n(k, r_s)$  are known by means of RPA [15, 30] (Appendix A). In the RPA treatment, the Kulik function  $G(x)$  appears [15], see Eqs. (A3)-(A5) and Fig. 1.  $G(x)$  will be used in the next section to build up a parametrized  $n(k, r_s)$  which satisfies Eqs. (3)-(8).

In the low-density or strongly correlated limit,  $r_s \rightarrow \infty$ , the electron gas undergoes Wigner crystallization (see, e.g., Ref. [43] and Appendix C). A simple model for the momentum distribution in such regime is reported in Appendix B.

### III. IMPROVED PARAMETRIZATION OF $n(k, r_s)$

The momentum distribution in terms of the Kulik function  $G(x)$  of Fig. 1 is parametrized as follows. For  $k < 1$  we use the ansatz

$$n_<(k, r_s) = n_0 - \frac{[n_0 - n_-]}{G(0)} G[x_<(k, r_s)], \quad (9)$$

while for  $k > 1$  we use

$$n_>(k, r_s) = \frac{n_+}{G(0)} G[x_>(k, r_s)], \quad (10)$$

with  $x_<(k, r_s)$  and  $x_>(k, r_s)$  equal to

$$x_<(k, r_s) = a \frac{\alpha r_s}{2\pi^2} \frac{G(0)}{[n_0 - n_-]} \frac{(1-k)}{\sqrt{4\alpha r_s/\pi}} + b \frac{\pi^2}{\alpha r_s} \sqrt{\frac{\pi}{3}} \frac{(1-\ln 2)}{F''(0)} \frac{[n_0 - n_-]}{G(0)} \frac{(1-k)^2}{k}, \quad (11)$$

$$x_>(k, r_s) = a \frac{\alpha r_s}{2\pi^2} \frac{G(0)}{n_+} \frac{(k-1)}{\sqrt{4\alpha r_s/\pi}} + \sqrt{\frac{3\pi(1-\ln 2)}{g_0}} \frac{n_+}{G(0)} \frac{\pi}{4\alpha r_s} (k-1)^4. \quad (12)$$

Here  $F''(0) = 17.968746$  [see Appendix A, Eq. (A1)], and the  $r_s$  dependence of  $a$ ,  $b$ ,  $n_0$ ,  $n_\pm$  and  $g_0$  is not explicitly shown for shortness. These constructions are such that  $n_<(k) \rightarrow n_0, n_-$  for  $k \rightarrow 0, 1^-$ , respectively, and  $n_>(k) \rightarrow n_+, 0$  for  $k \rightarrow 1^+, \infty$ , respectively. The behavior of the Kulik function for small and large arguments (see Appendix A) ensures the exact asymptotic expansion of Eqs. (5)-(8) near the centre, near the Fermi surface, and for large  $k$ .

The parameter  $a(r_s)$  determines the Fermi edge coefficient  $A(r_s)$  of the  $|1-k| \ln |1-k|$  term at the Fermi surface,

$$n(k \rightarrow 1^\pm, r_s) = n_\pm(r_s) \pm a(r_s) \left( \frac{\alpha r_s}{\pi} \right)^{1/2} \frac{1}{4} \left( \frac{\pi}{4} + \sqrt{3} \right) |1-k| \ln |1-k| + O(|1-k|). \quad (13)$$

The parameter  $b(r_s)$  determines the curvature  $B(r_s)$  of Eq. (8) at the centre,  $k = 0$ ,

$$n(k \rightarrow 0, r_s) = n_0(r_s) - \frac{\pi^4}{\alpha^2} \frac{F''(0)}{2} \left[ \frac{r_s}{b(r_s)} \right]^2 k^2 + O(k^4). \quad (14)$$

For small  $r_s$  (RPA - Appendix A) it is  $a(r_s \rightarrow 0) = 1$  and  $b(r_s \rightarrow 0) = 1$ .

In the preliminary version of Ref. [14], another (but similar) ansatz was introduced, and it was chosen  $b(r_s) = 1$ . Two different functions,  $a_<(r_s)$  and  $a_>(r_s)$ , for the coefficient of  $|1-k| \ln |1-k|$  at  $k = 1^-$  and  $k = 1^+$  were fixed by the sum rules of Eqs. (3) and (4) (with  $t_{\text{corr}}(r_s)$  from Ref. [23]). The values  $n_0(r_s)$  and  $n_\pm(r_s)$  were taken from the TY data (available for  $r_s = 1, \dots, 5$ ). The on-top value  $g_0(r_s)$  was taken from Ref. [10].

In our improved ansatz of Eqs. (9)-(12), we set  $a_<(r_s) = a_>(r_s) = a(r_s)$  (in agreement with Ref. [42]; also Figs. 7 and 8 of Ref. [14] confirm this), and we use again  $t_{\text{corr}}(r_s)$  from Ref. [23] and  $g_0(r_s)$  from Ref. [10]. Since we want to extend our results in the density range  $6 \leq r_s \leq 10$ , where there are no data available for  $n_0(r_s)$  and  $n_\pm(r_s)$ , we extract information

from the extreme low-density limit (Wigner crystal - see Appendix B), by following an oversimplified version of the idea presented in Ref. [44].

We first build  $n_0(r_s)$  by using a functional form which recovers the exact high-density limit, includes the Wigner crystal behavior as  $r_s \rightarrow \infty$ , and has some free parameters to be fitted to the TY data. The result is reported in Fig. 2, together with the high- and low-density curves. It is given by

$$n_0(r_s) = \frac{1 + t_1 r_s^2 + t_2 r_s^{5/2}}{1 + t_3 r_s^2 + t_4 r_s^{13/4}}, \quad (15)$$

with  $t_1 = 0.003438169$ ,  $t_2 = 0.00725313666$ ,  $t_3 = 0.014900367$ ,  $t_4 = 0.00113244364$  ( $t_1 - t_3$  agrees with the RPA value  $-(\frac{\alpha}{\pi^2})^2 4.1123 = -0.01146$ ). We then build the parameter  $b(r_s)$  by a simple interpolation between the high- and low-density limit of the curvature at the centre (see Fig. 3). The result is

$$b(r_s) = (1 + 0.0009376925 r_s^{13/4})^{1/2}. \quad (16)$$

Finally, the values at the Fermi edge,  $n_{\pm}(r_s)$ , and the coefficient of the infinite slope at the Fermi edge,  $a(r_s)$ , are obtained by fitting the TY values for  $n_{\pm}(r_s)$  while imposing the normalization and the kinetic energy [23] sum rules. The results are parametrized with the inclusion of the high- and low-density limits, and are equal to

$$n_{-}(r_s) = \frac{1 + v_1 r_s + v_2 r_s^2 + v_3 r_s^3}{1 + v_4 r_s + v_5 r_s^2 + v_6 r_s^3 + v_7 r_s^{15/4}}, \quad (17)$$

with  $v_1 = -0.0679793$ ,  $v_2 = -0.00102846$ ,  $v_3 = 0.000189111$ ,  $v_4 = 0.0205397$ ,  $v_5 = -0.0086838$ ,  $v_6 = 6.87109 \cdot 10^{-5}$ ,  $v_7 = 4.868047 \cdot 10^{-5}$  ( $v_1 - v_4$  agrees with the RPA value  $-\frac{\alpha}{2\pi^2} 3.3533 = -0.088519$ ), and

$$n_{+}(r_s) = \frac{q_1 r_s}{1 + q_2 r_s^{1/2} + q_3 r_s^{7/4}}, \quad (18)$$

with  $q_1 = 0.088519$  (from RPA),  $q_2 = 0.45$ ,  $q_3 = 0.022786335$ ;

$$a(r_s) = \frac{1 + p_1 r_s^{1/4} + p_2 r_s^{1/2}}{1 + p_3 r_s^{1/4} + p_4 r_s^{1/2} + p_5 r_s + p_6 r_s^6}, \quad (19)$$

with  $p_1 = -78.8682$ ,  $p_2 = -0.0989941$ ,  $p_3 = -68.5997$ ,  $p_4 = 38.1159$ ,  $p_5 = -17.6829$ ,  $p_6 = -0.01136759$ . Our parametrized  $n(k, r_s)$  breaks down at  $r_s \gtrsim 12$  [in the density range  $12 \lesssim r_s \lesssim 16$ ,  $n(k > 1, r_s)$  is no longer convex, and for  $r_s \gtrsim 16$  the unphysical result  $n_- < n_+$  is obtained when the sum rules of Eqs. (3) and (4) are imposed].

In the left panel of Fig. 4, we show the functions  $n_{\pm}(r_s)$ , together with the TY values, and the high and low-density limits (here the  $r_s \rightarrow \infty$  limit is considered to be the inflection point of the WC momentum distribution, see Eq. (B4)). As said, our model is only valid for  $r_s \lesssim 12$ , so that  $n_{-}(r_s)$  and  $n_{+}(r_s)$  at densities lower than  $r_s = 12$  are no more obtained from the constraints of Eqs. (3) and (4). Thus, the strange behavior of  $n_{-}(r_s)$  at  $r_s \sim 16$  does not affect our results. Also, the scheme presented here for the transition between the metallic and the extreme low-density region is oversimplified and must not be regarded as rigorous or reliable: we did not take into account the transition to the partially polarized electron gas (which affects the  $r_s \gtrsim 20$  densities [43] – see Appendix C), as well as many other features. However, our results seem to be reliable in the relevant density range  $r_s \lesssim 12$ , and the simple picture of the left panel of Fig. 4 is only a “naïve suggestion”. In the right panel of Fig. 4, we compare our parametrized  $z_F(r_s)$  with the TY results. In Fig. 5, we report the  $r_s$  dependence of the Fermi edge coefficient  $A(r_s)$ . Finally, in Fig. 6, we present in the left panel our parametrized  $n(k, r_s)$  for  $1 \leq r_s \leq 10$ , and in the right panel we compare our result with the TY  $n(k, r_s)$  and with the QMC data of Ref. [19] for  $r_s = 5$ .

#### IV. MOMENTS, CORRELATION ENTROPY, 1-MATRIX, AND CUMULANT EXPANSION

With the now available momentum distribution  $n(k, r_s)$ , its moments

$$\langle k^\nu \rangle = \int_0^\infty dk^3 n(k, r_s) k^\nu, \quad (20)$$

can be evaluated in addition to the normalization for  $\nu = 0$  and the kinetic energy for  $\nu = 2$  [Eqs. (3) and (4)]. They are shown in Fig. 7 for  $r_s = 3$  and 10, together with the  $r_s = 0$  (ideal Fermi gas) and with the WC result ( $r_s = 75$ ). The expression

$$(\Delta t)^2 = \frac{1}{(\alpha r_s)^4} [\langle k^4 \rangle - \langle k^2 \rangle^2] \quad (21)$$

(measured in ryd<sup>2</sup>) describes the fluctuation of the kinetic energy. The moments  $\langle k^2 \rangle$  and  $\langle k^4 \rangle$  determine the small- $x$  behavior of the 1-matrix, see Eq. (25).

In Ref. [45, 46], the entropy-like expression  $s(r_s) = -\langle \ln n(k, r_s) \rangle$  as a function of the interaction strength  $r_s$  has been used as a measure of the correlation strength [47]. Here the

expression

$$s_{\text{ph}}(r_s) = \int dk^3 (-1)\{n(k, r_s) \ln n(k, r_s) + [1 - n(k, r_s)] \ln[1 - n(k, r_s)]\} \quad (22)$$

is introduced as an alternative with the understanding that  $n(k, r_s)$  and  $1 - n(k, r_s)$  are the probabilities for the momentum state  $\underline{k}$  to be occupied (with spin up and spin down) and empty, respectively. The entropy of this probability ‘distribution’ is just the integrand of Eq. (22), and  $s_{\text{ph}}(r_s)$  is the sum of all these entropies. Notice its invariance under the exchange  $n(k, r_s) \leftrightarrow 1 - n(k, r_s)$ , which is referred to as particle-hole symmetry in the Reduced-Density-Matrix community. This symmetry is an intrinsic property of the correlation energy as a functional of the 1-matrix [48].  $s_{\text{ph}}(r_s)$  is plotted in Fig. 8. Another measure of the correlation strength is the correlation-tail normalization

$$n_{\text{corrtail}}(r_s) = \int_1^\infty dk^3 n(k, r_s), \quad (23)$$

also reported in Fig. 8. For large  $r_s$ , the Fermi edge disappears,  $z_F(r_s) = 0$ , and also any relict of it,  $A(r_s) = 0$ , then the inflexion point of  $n(k, r_s)$  vs.  $k$  may serve in Eq. (23) as the lower limit.

With  $n(k, r_s)$  also the (dimensionless) 1-matrix

$$f(x, r_s) = \int_0^\infty dk^3 \frac{\sin kx}{kx} n(k, r_s), \quad x = k_F |\underline{r} - \underline{r}'| \quad (24)$$

is available as the inverse of Eq. (2). It has the small- $x$  behavior

$$f(x \ll 1, r_s) = 1 - \frac{\langle k^2 \rangle}{3!} \cdot x^2 + \frac{\langle k^4 \rangle}{5!} \cdot x^4 - \frac{1}{5!} \frac{2}{9\pi} (\alpha r_s)^2 g_0(r_s) \cdot x^5 + O(x^6) \quad (25)$$

and the large- $x$  asymptotics (Friedel oscillations with reduced amplitudes)

$$f(x \gg 1, r_s) = -3 z_F(r_s) \frac{\cos x}{x^2} + 3 \frac{z_F(r_s) \sin x - \pi A(r_s) \cos x}{x^3} + O\left(\frac{1}{x^4}\right), \quad (26)$$

see Appendix D.  $A(r_s) = a(r_s) (\frac{\alpha r_s}{\pi})^{1/2} 0.63$  is the Fermi edge coefficient, the prefactor of the logarithmic term  $(k - 1) \ln |k - 1|$  in  $n(k \approx 1, r_s)$ . The factor 0.63 is the Kulik number 7.91, see Eq. (A6), divided by  $4\pi$ . In the inverse Fourier transform (2), the oscillatory terms of Eq. (26) do not affect the small- $k$  behavior of  $n(k, r_s)$ , because their average is zero. Since  $n(k \ll 1, r_s) = n_0(r_s) + O(k^2)$ , the large- $x$  behavior of the non-oscillatory  $f(x, r_s)$  is  $\propto 1/x^6$  or faster.  $f(x, r_s)$  is displayed in Fig. 9. One may partition  $n(k, r_s)$  and correspondingly

$f(x, r_s)$  in the following way:

$$\begin{aligned} n(k, r_s) &= z_F(r_s)\Theta(1-k) + n_1(k, r_s), \\ f(x, r_s) &= 3z_F(r_s) \frac{j_1(x)}{x} + f_1(x, r_s), \end{aligned} \quad (27)$$

where  $j_1(x) = (\sin x - x \cos x)/x^2$ .  $n_1(k, r_s)$  is a continuous function with  $n_1(1^-, r_s) = n_1(1^+, r_s)$  and an infinite slope at  $k = 1$ . Figure 10 shows  $n_1(k, r_s)$  and  $f_1(x, r_s)$  for  $r_s = 5$ .

The 1-matrix squared appears in the cumulant partitioning of the pair density,

$$g(x, r_s) = 1 - \frac{1}{2}|f(x, r_s)|^2 - h(x, r_s), \quad x = k_F r_{12}. \quad (28)$$

This defines the cumulant pair density  $h(x, r_s)$ , which is the diagonal of the above mentioned cumulant 2-matrix  $\chi(1|1', 2|2')$ . The spin-resolved version of Eq. (28) is

$$g_{\uparrow\uparrow}(x, r_s) = 1 - |f(x, r_s)|^2 - h_{\uparrow\uparrow}(x, r_s), \quad g_{\uparrow\downarrow}(x, r_s) = 1 - h_{\uparrow\downarrow}(x, r_s) \quad (29)$$

with  $g(x, r_s) = \frac{1}{2}[g_{\uparrow\uparrow}(x, r_s) + g_{\uparrow\downarrow}(x, r_s)]$  and  $h(x, r_s) = \frac{1}{2}[h_{\uparrow\uparrow}(x, r_s) + h_{\uparrow\downarrow}(x, r_s)]$ . Notice that the (generalized exchange or) Fock term  $|f(x, r_s)|^2$  appears only in the parallel-spin pair density and not in the antiparallel-spin pair density.  $g_{\uparrow\uparrow}(x, r_s)$  describes the Fermi hole (due to both Pauli and Coulomb repulsion) with  $g_{\uparrow\uparrow}(0, r_s) = h_{\uparrow\uparrow}(0, r_s) = 0$  and  $g_{\uparrow\downarrow}(x, r_s)$  describes the Coulomb hole (only due to the Coulomb repulsion) with  $g_{\uparrow\downarrow}(0, r_s) < 1$ . In addition to the above mentioned correlation-strength indices, the quantities  $h''_{\uparrow\uparrow}(0, r_s)$  measuring the on-top Fermi-hole curvature, and  $h_{\uparrow\downarrow}(0, r_s)$  measuring the on-top Coulomb hole are other ones.

From Eq. (26) it follows

$$|f(x \gg 1, r_s)|^2 = \frac{9}{2} \left[ \frac{z_F^2(r_s)}{x^4} + \frac{2\pi A(r_s)z_F(r_s)}{x^5} \right] (1 + \cos 2x) - 9 \frac{z_F^2(r_s)}{x^5} \sin 2x + O\left(\frac{1}{x^6}\right). \quad (30)$$

If this is inserted into Eq. (28), then the non-oscillatory terms,  $\frac{9z_F^2}{2x^4} + \frac{9\pi z_F A}{x^5}$ , are canceled by the asymptotics of  $h(x, r_s)$ , which follow from the sum-rule properties of the static structure factor  $S(q, r_s)$ , see Sec. V and Ref. [39]. The nominator of the oscillating  $1/x^5$  term can be written as

$$\sqrt{z_F^2(r_s) + \pi^2 A^2(r_s)} \sin(x - x_0(r_s)), \quad \tan x_0(r_s) = \frac{\pi A(r_s)}{z_F(r_s)}.$$

The on-top properties of  $g_{\uparrow\uparrow}(x \ll 1, r_s)$  and  $g_{\uparrow\downarrow}(x \ll 1, r_s)$  are determined by the coalescing cusp theorems [36, 49].

With Eq. (29), with the spin-resolved pair densities of Ref. [27], and with  $f(x, r_s)$  of this paper, the resulting cumulant pair densities  $h_{\uparrow\uparrow}(x, r_s)$  and  $h_{\uparrow\downarrow}(x, r_s)$  are plotted in Fig. 11. For small  $r_s$  ( $\ll 1$ ), our results agree with those of Ref. [12].

## V. STATIC STRUCTURE FACTOR, DENSITY FLUCTUATIONS, AND POTENTIAL ENERGY

The cumulant partitioning of Eq. (28) causes corresponding decompositions of all the quantities containing  $1 - g(x, r_s)$ . Such quantities are the static structure factor  $S(q, r_s)$ , the fluctuation  $\Delta N_\Omega(r_s)$  of the particle number in a fragment  $\Omega$ , and the potential energy  $v(r_s)$ .

So, the static structure factor is given by

$$S(q, r_s) = 1 - \frac{1}{2}\tilde{n}^2(q, r_s) - \tilde{h}(q, r_s) \quad (31)$$

with the (generalized exchange or) Fock component

$$\begin{aligned} \tilde{n}^2(q, r_s) &= \alpha^3 \int_0^\infty dx^3 \frac{\sin qx}{qx} |f(x, r_s)|^2 \\ &= \int_0^\infty dk^3 n(k, r_s) \int_{-1}^{+1} d\zeta n(\sqrt{k^2 + q^2 - 2kq\zeta}, r_s) \end{aligned} \quad (32)$$

(from which it follows that  $\tilde{n}^2(q, r_s)$  has a discontinuity in its second derivative at  $q = 2$ ) and the cumulant component

$$\tilde{h}(q, r_s) = \alpha^3 \int_0^\infty dx^3 \frac{\sin qx}{qx} h(x, r_s), \quad (33)$$

which is simply the Fourier transform of the cumulant pair density  $h(x, r_s)$ . In Eq. (32) the convolution theorem has been applied.  $\tilde{n}^2(q, r_s)$  is related to the probability of finding a pair of electrons with given relative momentum  $q$  [10, 11].

Notice that the sum rule  $S(q \rightarrow 0, r_s) = 0$  is equivalent to the sum rule

$$\alpha^3 \int_0^\infty dx^3 h(x, r_s) = \int_0^\infty dk^3 n(k, r_s) [1 - n(k, r_s)]. \quad (34)$$

The l.h.s. equals  $\tilde{h}(0, r_s)$  and the r.h.s. equals  $1 - \frac{1}{2}\tilde{n}^2(0, r_s)$ . It was already P.-O. Löwdin who has asked what meaning the r.h.s. has [50]. According to Eq. (34), it fixes the normalization of the cumulant pair density  $h(x, r_s)$  and is another particle-hole symmetric measure of

the correlation strength; it is also reported in Fig. 8. Eq. (34) is sometimes called perfect screening sum rule or charge neutrality condition.

For non-interacting electrons ( $r_s = 0$ ), the cumulant part vanishes,  $\tilde{h}(q, r_s) = 0$ , and the Fock part  $S_F(q, r_s)$  simply yields

$$S_0(q) = \frac{q}{2} \left[ \frac{3}{2} - \frac{1}{2} \left( \frac{q}{2} \right)^2 \right] \Theta \left( 1 - \frac{q}{2} \right) + \Theta \left( \frac{q}{2} - 1 \right) \quad (35)$$

with the linear small- $q$  behavior  $3q/4$ . For interacting electrons ( $r_s \neq 0$ ) the small- $q$  sum rule [41, 51]

$$S(q \ll 1, r_s) = \frac{1}{2(\alpha r_s)^2 \omega_{\text{pl}}(r_s)} \cdot q^2 + O(q^4), \quad (36)$$

and the large- $q$  sum rule [49]

$$S(q \gg 1, r_s) = 1 - \frac{8}{3\pi} \alpha r_s g_0(r_s) \cdot \frac{1}{q^4} + O \left( \frac{1}{q^6} \right) \quad (37)$$

hold.  $\omega_{\text{pl}}^2(r_s) = 4\pi e^2 \rho/m = 3/r_s^3$  a.u. defines the plasma frequency. Question (in Appendix C it is attempted to answer it in terms of the inflexion-point trajectory): When  $r_s \rightarrow 0$ , how does the quadratic small- $q$  behavior of Eq. (36) turn into the linear behavior of Eq. (35)?

The non-idempotency and the singularities of  $n(k, r_s)$  determine the small- $q$  behavior of  $S_F(q, r_s) = 1 - \frac{1}{2} \tilde{n}^2(q, r_s)$ ,

$$S_F(q \ll 1, r_s) = S_F(0, r_s) + \frac{3}{4} z_F^2(r_s) q - A(r_s) z_F(r_s) q^2 \ln q + O(q^2), \quad (38)$$

as shown in Appendix E. Notice that  $S_F(0, r_s)$  is equal to the r.h.s. of Eq. (34). In Fig. 12, we report  $S_F(q, r_s)$  for the ideal gas ( $r_s = 0$ ), for  $r_s = 5$ , and in the WC limit.

Eq. (38), together with the sum rule of Eq. (36), allows to extract the large- $x$  behavior of  $h(x, r_s)$ . Namely, because of Eq. (36),  $\tilde{h}(q, r_s)$  must cancel both the linear and the  $q^2 \ln q$  term of  $\tilde{n}^2(q, r_s)$ . This implies that the large- $x$  behavior of the oscillation-averaged  $\langle h(q, r_s) \rangle$  is:

$$\langle h(x \gg 1, r_s) \rangle = -\frac{9}{4} \frac{z_F^2(r_s)}{x^4} - \frac{9}{2} \frac{\pi A(r_s) z_F(r_s)}{x^5} + O \left( \frac{1}{x^6} \right). \quad (39)$$

In Eq. (28) this cancels the non-oscillatory terms of  $\frac{1}{2} |f(x, r_s)|^2$ .

If we consider within the uniform electron gas a certain fragment  $\Omega$  (e.g., a sphere of radius  $R$ ) containing on average  $N_\Omega = \Omega/(4\pi r_s^3/3) = (R/r_s)^3$  electrons, and ask for the

particle-number fluctuation  $\Delta N_\Omega$  then the answer is [52, 53]

$$\begin{aligned} \frac{(\Delta N_\Omega)^2}{N_\Omega} &= 1 - \frac{(\alpha r_s)^6}{N_\Omega} \int_\Omega d^3 x_1 \int_\Omega d^3 x_2 \left[ \frac{1}{2} |f(x, r_s)|^2 + h(x, r_s) \right] \\ &= 1 - \frac{(\alpha r_s)^6}{N_\Omega} \frac{3}{8\pi} \int d^3 q \left| \int_\Omega d^3 x e^{i\vec{q}\cdot\vec{x}} \right|^2 \left[ \frac{1}{2} \tilde{n}^2(q, r_s) + \tilde{h}(q, r_s) \right]. \end{aligned} \quad (40)$$

Again one may ask how differently the Fock and the cumulant parts contribute to their sum and to the conclusion ‘correlation suppresses fluctuations’ [1, 53]. In the case of a sphere  $\Omega = 4\pi R^3/3$ , the term in the modulus in Eq. (40) is just  $\Omega 3j_1(qR)/(qR)$ , so that the Fock term yields

$$\left[ \frac{(\Delta N_\Omega)^2}{N_\Omega} \right]_{\text{F}} = 1 - \frac{3}{2} \pi^2 \Omega (\alpha r_s)^9 \int_0^\infty dq^3 \left[ \frac{3 j_1(qR)}{qR} \right]^2 \tilde{n}^2(q, r_s). \quad (41)$$

Also, the potential energy  $v(r_s)$  consists of a Fock and a cumulant part [7]:

$$\begin{aligned} v(r_s) &= -\frac{\alpha^2}{r_s} \int_0^\infty dx^3 \left[ \frac{1}{2} |f(x, r_s)|^2 + h(x, r_s) \right] \frac{1}{x} \\ &= -\frac{\alpha^2}{r_s} \frac{3}{2} \int_0^\infty dq^3 \left[ \frac{1}{2} \tilde{n}^2(q, r_s) + \tilde{h}(q, r_s) \right] \frac{1}{q^2} \end{aligned} \quad (42)$$

(in ryd). The Fock part can also be written as [7]

$$v_{\text{F}}(r_s) = -\frac{3}{2\pi\alpha r_s} \int_0^\infty dk n(k, r_s) \int_0^\infty dk' n(k', r_s) k k' \ln \frac{k+k'}{|k-k'|}. \quad (43)$$

In lowest order, with  $n(k, r_s) \rightarrow \theta(1-k)$ , Eq. (43) yields  $-3/(2\pi\alpha r_s)$ . The logarithmic term of  $v(r_s \rightarrow 0)$  arises from  $v_{\text{C}}(r_s)$ , not from  $v_{\text{F}}(r_s)$  [12].

## VI. SUMMARY AND OUTLOOK

In Ref. [14], it was shown that the convex Kulik function  $G(x)$ , decorated with appropriate prefactors and with an appropriate inhomogeneous scaling of its argument, reproduces the momentum distribution  $n(k, r_s)$  of the unpolarized uniform electron gas of density  $\rho = 3/4\pi r_s^3$  in the metallic-density regime  $r_s \in [1, 6]$ . The  $r_s$ -functions  $n(0, r_s)$ ,  $n(1^\pm, r_s)$ , the on-top pair density  $g(0, r_s)$ , and the kinetic energy  $t(r_s)$  form the input for such construction. In this work, we improved the parametrization of  $n(k, r_s)$  via the Kulik function, and we extended it up to  $r_s \lesssim 12$ , including the high-density regime [Eqs. (9)–(12), and Fig. 6].

The Fourier transform of  $n(k, r_s)$  yields the one-body reduced density matrix  $f(x, r_s)$  (Figs. 9 and 10), with large  $x$ -oscillations arising from the Fermi gap  $z_{\text{F}}(r_s)$  and the Fermi

edge coefficient  $A(r_s)$ , the prefactor of the logarithmic term in  $n(k \approx 1, r_s)$ , which is included in our parametrization for the first time (Fig. 5). Several measures of the correlation strength have been discussed (Fig. 8). With reliable models for the pair density,  $g(x, r_s)$ , the cumulant pair density  $h(x, r_s) = 1 - \frac{1}{2}|f(x, r_s)|^2 - g(x, r_s)$  has been extracted (Fig. 11), as a prestep of its diagonalization in terms of cumulant geminals (analog with the diagonalization of the pair density in terms of Overhauser geminals). Future work also includes the generalization to the partially polarized gas. In this case, with  $\zeta = (N_\uparrow - N_\downarrow)/N$ , one has to consider different cases. For spin polarization  $\zeta$  between 0 and 1, two momentum distributions are to be described,  $n_\uparrow(k, r_s, \zeta)$  for the spin-up electrons and  $n_\downarrow(k, r_s, \zeta)$  for the spin-down electrons. So far, only the input data  $g_0(r_s, \zeta)$  [10] and  $t(r_s, \zeta)$  [23] are available in this more general case.

A small **Fortran** subroutine, aimed at the evaluation of our parametrized  $n(k, r_s)$ , is available upon request to [gp.giorgi@caspur.it](mailto:gp.giorgi@caspur.it).

### Acknowledgments

The authors thank Y. Takada for providing the data for  $n(0, r_s)$  and  $n(1^\pm, r_s)$ , and J. Cioslowski and G. Diener for helpful discussions. One author (P.G.-G.) gratefully acknowledges hospitality at the Max Planck Institut für Physik komplexer Systeme of Dresden (Germany), the other author (P.Z.) thanks P. Fulde for supporting this work.

### APPENDIX A: RANDOM PHASE APPROXIMATION

In RPA it is  $n(k, r_s) = 1 - (\alpha r_s/\pi^2)^2 H(k, 1)$  for  $k < 1$  and  $(\alpha r_s/\pi^2)^2 H(k, 1)$  for  $k > 1$ , where

$$H(x < 1, y) = \frac{1}{x} \left\{ \int_{1-x}^{1+x} \frac{dq}{q} \int_0^\infty du \left[ \frac{\frac{1-x^2}{2q}}{(\frac{1-x^2}{2q})^2 + u^2} - \frac{\frac{q}{2} + x}{(\frac{q}{2} + x)^2 + u^2} \right] \frac{Q(q, u)}{q^2 + y \frac{\alpha r_s}{\pi^2} Q(q, u)} \right. \\ \left. + \int_{1+x}^\infty \frac{dq}{q} \int_0^\infty du \left[ \frac{\frac{q}{2} - x}{(\frac{q}{2} - x)^2 + u^2} - \frac{\frac{q}{2} + x}{(\frac{q}{2} + x)^2 + u^2} \right] \frac{Q(q, u)}{q^2 + y \frac{\alpha r_s}{\pi^2} Q(q, u)} \right\}, \\ H(x > 1, y) = \frac{1}{x} \int_{x-1}^{x+1} \frac{dq}{q} \int_0^\infty du \left[ \frac{\frac{x^2-1}{2q}}{(\frac{x^2-1}{2q})^2 + u^2} - \frac{x - \frac{q}{2}}{(x - \frac{q}{2})^2 + u^2} \right] \frac{Q(q, u)}{q^2 + y \frac{\alpha r_s}{\pi^2} Q(q, u)}$$

and

$$Q(q, u) = 2\pi \left\{ 1 + \frac{1 + u^2 - q^2/4}{2q} \ln \frac{(1 + q/2)^2 + u^2}{(1 - q/2)^2 + u^2} - u \left[ \arctan \frac{1 + q/2}{u} + \arctan \frac{1 - q/2}{u} \right] \right\}$$

[15, 30]. For small or large  $k$  (far from the Fermi edge) it is  $H(k, 1) \rightarrow F(k)$  with  $F(k) = H(k, 0)$ .  $F(k)$  has the small and large  $k$  properties

$$F(k \ll 1) = 4.112335 + 8.984373 \cdot k^2 + O(k^4) \quad (\text{A1})$$

and

$$F(k \gg 1) = \frac{8\pi^2}{9} \cdot \frac{1}{k^8} + O\left(\frac{1}{k^{10}}\right), \quad (\text{A2})$$

respectively [54, 55]. The coefficient of  $1/k^8$  is 8.77298.

For  $k$  near the Fermi edge it is [54, 55]

$$H(k, 1) \rightarrow \frac{\pi^2}{2\alpha r_s} \frac{1}{k^2} G\left(\frac{|k - 1|}{\sqrt{4\alpha r_s/\pi}}\right) \quad (\text{A3})$$

with

$$G(x) = \int_0^\infty du (-1) \frac{R'(u)}{R(u)} \cdot \frac{u}{u + y} \cdot (-1) \frac{R(u) - R(y)}{u - y} \Big|_{y=x/\sqrt{R(u)}} \quad (\text{A4})$$

and

$$R(u) = 1 - u \arctan \frac{1}{u}. \quad (\text{A5})$$

$G(x)$  has the small- $x$  behavior [15]

$$G(x \ll 1) = G(0) + \left[ \pi \left( \frac{\pi}{4} + \sqrt{3} \right) \cdot x + O(x^2) \right] \ln x + O(x) \quad (\text{A6})$$

with

$$G(0) = \int_0^\infty du (-1) \frac{R'(u)}{R(u)} \cdot \arctan \frac{1}{u} \approx 3.353337. \quad (\text{A7})$$

The coefficient of  $x \ln x$  is 7.908799 (the Kulik number).  $G(x)$  has the large- $x$  behavior

$$G(x \gg 1) = \frac{\pi}{6} (1 - \ln 2) \cdot \frac{1}{x^2} + O\left(\frac{1}{x^4}\right). \quad (\text{A8})$$

The coefficient of  $1/x^2$  is 0.160668 (the Macke number). The Kulik function  $G(x)$  is shown in Fig. 1.

## APPENDIX B: THE MOMENTUM DISTRIBUTION OF THE WIGNER CRYSTAL

In the low-density (large  $r_s$ ) or strongly correlated limit, the electrons localize [43] and form a ferromagnetic body-centered cubic lattice with an electrostatic (or Madelung) energy of  $-1.792/r_s$  ryd [56]. The next term,  $+2.65/r_s^{3/2}$  ryd, describes the coupled harmonic zero-temperature motion in lowest order [57, 58, 59]. To estimate the corresponding  $n(k, r_s)$ , we define with  $3\hbar\omega/2 = 2.65/r_s^{3/2}$  (in ryd, or  $\omega = 0.88/r_s^{3/2}$  in a.u.) the frequency of independent oscillating electrons (Einstein model). So, from the momentum distribution of the harmonic-oscillator ground state it follows

$$n(k, r_s \rightarrow \infty) = \frac{4\pi}{3} \frac{1}{(\pi\omega/k_F^2)^{3/2}} e^{-\frac{k^2}{\omega/k_F^2}} \quad (B1)$$

see [60, 61], and [32], p. 19. Note that  $k$  is dimensionless (measured in units of  $k_F$ ) and that  $\omega/k_F^2 = 0.88 \cdot \alpha^2 r_s^{1/2} = 0.24 \cdot r_s^{1/2}$ . In Ref. [61], the factor 1 is used instead of 0.88.  $n(k, r_s \rightarrow \infty)$  is correctly normalized and yields with Eq. (4) the kinetic energy (in ryd)

$$t(r_s \rightarrow \infty) = \frac{1}{2} \cdot \frac{2.65}{r_s^{3/2}} + \dots \quad (B2)$$

as it should. The corresponding potential energy is

$$v(r_s \rightarrow \infty) = -\frac{1.792}{r_s} + \frac{1}{2} \cdot \frac{2.65}{r_s^{3/2}} + \dots \quad (B3)$$

The inflection-point trajectory with  $r_s$  as parameter is described by (see left panel of Fig. 4)

$$k_{\text{infl}}(r_s) = (\omega/(2k_F^2))^{1/2} = 0.35 \cdot r_s^{1/4}, \quad n_{\text{infl}}(r_s) = \frac{4\pi}{3} \frac{e^{-1/2}}{(\pi\omega/k_F^2)^{3/2}} = \frac{3.88}{r_s^{3/4}}. \quad (B4)$$

The region  $k > k_{\text{infl}}$  (maybe to be referred to as correlation tail) contributes to the normalization the constant amount

$$\int_{k_{\text{infl}}}^{\infty} dk^3 n(k, r_s) = \text{Erf}\left(\frac{1}{\sqrt{2}}\right) - \sqrt{\frac{2}{\pi}} = 0.80. \quad (B5)$$

From Eq. (B1) it follows for  $n(0, r_s \rightarrow \infty)$

$$n_0(r_s \rightarrow \infty) = \frac{4}{3\pi^{1/2}} \left( \frac{1}{0.24r_s^{1/2}} \right)^{3/2} = \frac{6.40}{r_s^{3/4}}, \quad (B6)$$

see Fig. 2; and for the curvature at the centre (the coefficient of  $k^2$ )

$$-\frac{4}{3\pi^{1/2}} \frac{1}{(0.88\alpha^2 r_s^{1/2})^{5/2}} = -\frac{26.71}{r_s^{5/4}}, \quad (B7)$$

see Fig. 3.

A more refined treatment takes into account that in harmonic approximation there are two transversal branches of harmonic lattice vibrations,  $\omega_{t_{1,2}}(\underline{q}, r_s)$ , and one longitudinal branch  $\omega_l(\underline{q}, r_s)$  in the face-centred cubic Brillouin zone, satisfying the sum rule  $\omega_{t_1}^2(\underline{q}, r_s) + \omega_{t_2}^2(\underline{q}, r_s) + \omega_l^2(\underline{q}, r_s) = \omega_{\text{pl}}^2(r_s)$ . For  $\underline{q} = 0$  it is  $\omega_{t_{1,2}}(0, r_s) = 0$  and therefore  $\omega_l(0, r_s) = \omega_{\text{pl}}(r_s)$ . But also in this case the virial theorem holds and assuming that  $n(k, r_s)$  is a Gauß distribution, then Eq. (B1) turns out again.

### APPENDIX C: PHASES, PHASE TRANSITIONS, AND TRAJECTORIES

A more sophisticated treatment needs to take into account the different zero-temperature phases and phase transitions, which the electron system passes through when the interaction strength  $r_s$  grows from  $r_s = 0$  (no interaction) to  $r_s \rightarrow \infty$  (Wigner crystal). Namely, the QMC calculations of Ortiz, Harris, and Ballone [43] show the following (with UPEG = unpolarized electron gas, PPEF = partially polarized electron fluid, FMEF = ferromagnetic electron fluid, FMWC = ferromagnetic Wigner crystal):

UPEG  $-(r_1) \rightarrow$  PPEF  $-(r_2) \rightarrow$  FMEF  $-(r_3) \rightarrow$  FMWC

with  $r_1 \approx 20$ ,  $r_2 \approx 40$ , and  $r_3 \approx 65$  and with the spin polarization  $\zeta = (\rho_\uparrow - \rho_\downarrow)/\rho$  being 0 for  $r_s \leq r_1$  and growing up to 1 for  $r_s \geq r_2$ . The two equal momentum distributions  $n_\uparrow(k, r_s)$  and  $n_\downarrow(k, r_s)$  with the same Fermi wave number  $k_{F\uparrow} = k_{F\downarrow} = k_F$  for  $r_s < r_1$ , change at  $r_s = r_1$  into two different momentum distributions,  $n_\uparrow(k, r_s)$  for the majority and  $n_\downarrow(k, r_s)$  for the minority, with two different Fermi wave numbers, the larger,  $k_{F\uparrow} = (1 + \zeta)^{1/3}k_F$ , and the smaller,  $k_{F\downarrow} = (1 - \zeta)^{1/3}k_F$ . At  $r_s \leq r_2$ , the spin-down Fermi body disappears and only the spin-up Fermi body survives. Finally, at  $r_s = r_3$  the FMEF crystallizes to the FMWC. Now the question arises: At which critical  $r_s$  values,  $r_z$  and  $r_a$ , the Fermi gap  $z_F(r_s)$  and the Fermi edge parameter  $a(r_s)$ , disappear, respectively? When  $r_z = r_1$  and  $r_a = r_2$  (as one possible scenario), then only the phase UPEG would be a Fermi liquid with a non-vanishing Fermi gap  $z_F(r_s) \neq 0$ , while the phases PPEF and FMEF would be non-Fermi liquids with no Fermi gap but with an infinite slope at  $k_{F\uparrow}$  [non-vanishing Fermi edge coefficient  $A(r_s)$ ]. Then, the FMEF phase would be a ‘normal’ quantum liquid with a non-infinite slope at the inflection point of  $n(k, r_s)$  vs.  $k$ . In the light of such a more complicated situation our treatment of Sec. III is only a rather rough estimate.

Other points to discuss are the followings. The static structure factor  $S(q, r_s)$  turns from the quadratic small- $q$  behavior (40) for  $r_s > 0$  to the linear behavior (36) for  $r_s = 0$ . Possibly, the  $r_s$ -dependent inflection point of  $S(q, r_s)$  vs.  $q$  moves with  $r_s \rightarrow 0$  downward to the origin, see Fig. 13. So, with  $r_s \rightarrow 0$  the linear behavior at the inflection point is transported to  $q = 0, S(0, 0) = 0$ .

Similarly, the  $k$ -dependent inflection point of  $n(k, r_s)$  vs.  $r_s$  moves from its position for  $k = 0$  (which is the inflection point of  $n_0(r_s)$ ) upward to  $r_s = 0, n_-(r_s) = 1$  for  $k \rightarrow 1^-$ .

In the case of  $k^8 n(k, r_s)$  vs.  $r_s$  for  $k = 1^+$  to  $k \rightarrow \infty$  the linear small- $r_s$  behavior becomes more and more flat and vanishes finally for  $k \rightarrow \infty$ . So, the next term  $\sim r_s^2$  rises to be the leading term.

## APPENDIX D: 1-MATRIX NEAR THE DIAGONAL AND FAR FROM IT

The equation  $\gamma(1|1') = \rho \delta_{\sigma_1 \sigma'_1} f(k_F |\underline{r}_1 - \underline{r}'_1|)$  defines the dimensionless 1-matrix  $f(x)$ . Its small- $x$  behavior of Eq. (25) follows from the large- $k$  behavior of  $n(k)$  [Eq. (5)]. Namely, with  $\sin y/y = 1 - y^2/3! + y^4/5! - \dots$  and with the integrability of  $n(k)k^2 k^\nu$  for  $\nu = 0, \dots, 4$  it is

$$f^{(\nu)}(0) = \int_0^\infty dk^3 n(k) k^\nu \left( \frac{d}{dy} \right)^\nu \frac{\sin y}{y} \Big|_{y=0}, \quad (\text{D1})$$

which yields the first three terms of Eq. (25). Here  $f^{(\nu)}(0) = (\frac{d}{dx})^\nu f(x)|_{x=0}$ .

Because  $n(k)k^2 k^5$  is non-integrable, one has to compute  $f^{(5)}(0)$  with the Kimball procedure [49, 62], which defines by

$$n(k) = \frac{c}{(1+k^2)^4} + \mathcal{N}(k), \quad c = \frac{8}{9\pi^2} (\alpha r_s)^2 g_0(r_s) \quad (\text{D2})$$

a stronger (namely  $\sim 1/k^{10}$  for  $k \rightarrow \infty$ ) decaying function  $\mathcal{N}(k)$ , so that  $\mathcal{N}(k)k^2 k^5$  is now integrable, yielding 0 because of  $(d/dy)^5 \sin y/y|_{y=0} = 0$ . Thus

$$f^{(5)}(0) = \left( \frac{d}{dy} \right)^5 p(x) \Big|_{x=0} \quad (\text{D3})$$

with

$$p(x) = c \int_0^\infty \frac{dk^3}{(1+k^2)^4} \frac{\sin kx}{kx} = c \frac{\pi}{32} (3 + 3x + x^2) e^{-x}. \quad (\text{D4})$$

It follows

$$f^{(5)}(0) = -c \frac{\pi}{4} = -\frac{2}{9\pi} (\alpha r_s)^2 g_0(r_s), \quad (\text{D5})$$

q.e.d.

The large- $x$  behavior (26) follows from Eq. (24) by partial integration. Thereby the discontinuities of  $n(k, r_s)$  at  $k \approx 1$  appear. They determine the amplitudes of the Friedel oscillations:

$$f(x, r_s) = -z_F(r_s) \frac{3 \cos x}{x^2} + z_F(r_s) \frac{3 \sin x}{x^3} + f_1(x, r_s) \quad (\text{D6})$$

with

$$\begin{aligned} f_1(x \gg 1, r_s) &= -A(r_s) \frac{3}{x^3} \{ [\frac{\pi}{2} + \text{Si}(x)] \cos x - \text{Ci}(x) \sin x \} + O\left(\frac{1}{x^4}\right) \\ &= -A(r_s) \pi \frac{3 \cos x}{x^3} + O\left(\frac{1}{x^4}\right). \end{aligned} \quad (\text{D7})$$

$z_F(r_s)$  is the Fermi gap and  $A(r_s)$  is the Fermi edge coefficient.

## APPENDIX E: FOCK COMPONENT OF THE STATIC STRUCTURE FACTOR AT SMALL- $q$

According to the definition of Eq. (32), the oscillations of  $|f(x \gg 1, r_s)|^2$  [see Eq. (30)] only affect the discontinuities in  $\tilde{n}^2(q, r_s)$  and in its derivatives at  $q = 2$ , while the small- $q$  behavior of  $\tilde{n}^2(q, r_s)$  is only affected by the oscillation-averaged part of  $|f(x, r_s)|^2$ , i.e., by

$$\langle f^2(x \gg 1, r_s) \rangle = \frac{9}{2} \frac{z_F(r_s)}{x^4} + 9 \frac{\pi A(r_s) z_F(r_s)}{x^5} + O\left(\frac{1}{x^6}\right). \quad (\text{E1})$$

Following the procedure of Kimball [49, 62] we define a function  $\mathcal{F}(x)$  by

$$\langle f^2(x, r_s) \rangle = \mathcal{F}(x) + \frac{9}{2} \frac{z_F(r_s)}{(1+x^2)^2} + 9 \frac{\pi A(r_s) z_F(r_s)}{(1+x)^5}, \quad (\text{E2})$$

so that  $\mathcal{F}(x \rightarrow \infty) \propto 1/x^6$ . Then, the second term will give the coefficient of the linear term in  $\tilde{n}^2(q, r_s)$ , while the third term will give the coefficient of a term  $\propto q^2 \ln q$ . By carrying out the calculations one obtains Eq. (38), q.e.d. .

---

[1] Fulde P 1991 (3<sup>rd</sup> enlarged edition 1995) *Electron Correlation in Molecules and Solids* (Springer: Berlin)

- [2] Bartlett R J 2001 *Chemistry for the 21st Century* (Wiley: Weinheim), p. 271
- [3] Davidson E R 1976 *Reduced Density Matrices in Quantum Chemistry* (Academic Press: New York)
- [4] Erdahl R and Smith V H Jr eds 1987 *Density Matrices and Density Functionals* (Reidel: Dordrecht)
- [5] Coleman A J and Yukalov V I 2000 *Reduced Density Matrices* (Springer: Berlin)
- [6] Cioslowski J ed 2000 *Many Electron Densities and Reduced-Density Matrices* (Kluwer/Plenum: New York)
- [7] Ziesche P 1992 *Solid State Commun.* **82** 597
- [8] Ziesche P 2000 *Cumulant Expansions of Reduced Densities, Reduced Density Matrices, and Green's Functions* in Ref. [6], p. 33
- [9] Overhauser A W 1995 *Can. J. Phys.* **73** 683
- [10] Gori-Giorgi P and Perdew J P 2001 *Phys. Rev. B* **64** 155102
- [11] Davoudi B, Polini M, Asgardi R, and Tosi M P *cond-mat/0201423*
- [12] Ziesche P 2002 *Int. J. Quantum Chem.* **88**, in press (Published Online: 12 Mar 2002). - Therein  $O(x^6 \ln x)$  after Eq. (3.3) is to be replaced by  $-\frac{1}{5!} \frac{2}{9\pi} (\alpha r_s)^2 g(0, r_s) \cdot x^5 + O(x^6)$ , see Eq. (25). Besides Eq. (3.23) should read  $h_{\uparrow\uparrow}'''(0) = \frac{3}{2} \alpha r_s [2f''(0) + h''(0)]$  and instead of 'the cusp theorems are contained ... cusp theorems.' read 'the first cusp theorem is contained only in the cumulant PD  $h_{\uparrow\downarrow}(x)$ . The 1-body quantities  $n(k)$  or  $f(x)$  do not contribute to the first cusp theorem.'
- [13] Ziesche P 2002 in *Electron Correlations and Materials Properties II* ed. A. Gonis, N. Kioussis, and M. Ciftan (Kluwer/Plenum: New York), in press
- [14] Ziesche P 2002 *phys. stat. sol. (b)* in press
- [15] Kulik I O 1961 *Z. Eksp. Teor. Fiz.* **40**, 1343 [*Sov. Phys. JETP* **13**, 946]
- [16] March N H 1958 *Phys. Rev.* **110** 604
- [17] Takada Y and Yasuhara H 1991 *Phys. Rev. B* **44** 7879
- [18] Takada Y 1992, private communication on the basis of the method described in Ref. [17]
- [19] Ortiz G and Ballone P 1994/1997 *Phys. Rev. B* **50** 1391; Erratum: B **56**, 9970
- [20] Senatore G, Moroni S, and Ceperley D M 1995 in: *Physics on strongly coupled plasmas* ed W. D. Kraeft (World Scientific: Singapore), p.429.
- [21] Barbiellini B and Bansil A 2001 *J. Phys. Chem. Solids* **62** 2181
- [22] Farid B, Heine V, Hengel G E, Robertson I J 1993 *Phys. Rev B* **48** 11602

- [23] Perdew J P and Wang Y 1992 *Phys. Rev. B* **45** 13244
- [24] The infinite slope at the Fermi edge was previously taken into account in a study of the momentum distribution of  $^3\text{He}$  [31]; the authors also extracted the Fermi edge coefficient  $A$  of Eqs. (6) and (7) from QMC simulations. At the equilibrium density, corresponding to  $r_s = 4.62$ , they found  $A = 0.06(2)$ .
- [25] Cioslowski J, private communication
- [26] Perdew J P and Wang Y 1992 *Phys. Rev. B* **46** 12947; 1997 *Phys. Rev. B* **56** 7018
- [27] Gori-Giorgi P, Sacchetti F, and Bachelet G B 2000 *Phys. Rev. B* **61** 7353
- [28] Gori-Giorgi P and Perdew J P 2002, unpublished
- [29] Gori-Giorgi P, Sacchetti F, and Bachelet G B 2000 *Physica A* **280** 199
- [30] Daniel E and Vosko S H 1960 *Phys. Rev.* **120** 2041
- [31] Moroni S, Senatore G, and Fantoni S 1997 *Phys. Rev. B* **55** 1040
- [32] Ziesche P and Lehmann G eds 1983 *Ergebnisse in der Elektronentheorie der Metalle* (Akademie/Springer: Berlin)
- [33] Macke W 1950 *Z. Naturforsch.* **A5**, 192
- [34] Gell-Mann M and Brueckner K A 1957 *Phys. Rev.* **106** 364
- [35] Onsager L, Mittag L and Stephen M J 1966 *Ann. Phys. (Leipzig)* **18** 71
- [36] Kimball J C 1975 *J. Phys. A* **8** 1513
- [37] Yasuhara H and Kawazoe Y 1976 *Physica A* **85** 416
- [38] Geldart D J W 1967 *Can. J. Phys.* **45** 3139
- [39] Kimball J C 1976 *Phys. Rev. B* **14** 2371
- [40] Comparison of Eq. (A2) with Eq. (5) shows that RPA fails to reproduce the correct large- $k$  expansion of  $n(k, r_s)$ : for small- $r_s$ , instead of having  $k^8 n(k) \rightarrow \frac{8}{9} \pi^2 (\alpha r_s^2) [\frac{1}{2} + O(r_s)]$ , RPA yields  $k^8 n(k) \rightarrow \frac{8}{9} \pi^2 (\alpha r_s^2) [1 + O(r_s)]$ . The lowest order exchange diagram [35] repairs this, see Figs. 1c and 1f of Ref. [12]
- [41] Pines D and Nozières P 1966 *Theory of Quantum Liquids* (Benjamin: New York).
- [42] Sartor R and Mahaux C 1980 *Phys. Rev. C* **21** 1546
- [43] Ortiz G, Harris M, and Ballone P 1999 *Phys. Rev. Lett.* **82** 5317
- [44] Seidl M, Perdew J P, and Kurth S 2000 *Phys. Rev. A* **62** 012502, *Phys. Rev. Lett.* **84** 5070
- [45] Ziesche P 1995 *Int. J. Quantum Chem.* **56** 363
- [46] Ziesche P 2000 *J. Mol. Structure (Theochem)* **527** 35 and references therein. Therein factors

1/2 are erroneously incorporated in the definition of  $g_{\uparrow\uparrow}(x)$  and  $g_{\uparrow\downarrow}(x)$  such that  $g_{\uparrow\uparrow}(0) = g_{\uparrow\downarrow}(0) = 1/2$  instead of 1.

- [47]  $s(0) = 0$  together with the Macke formula  $\epsilon_{\text{corr}}(r_s \ll 1) = 0.06218 \ln r_s + O(r_s^0)$  obviously contradicts Collins' conjecture "correlation entropy  $\sim$  correlation energy" [45, 63].
- [48] Ruskai M B 1970 *J. Math. Phys.* **11** 3218
- [49] Kimball J C *Phys. Rev.* 1973 **A7** 1648
- [50] Löwdin P-O 1959 *Adv. Chem. Phys.* **2** 207
- [51] Iwamoto N 1986 *Phys. Rev. A* **33** 1940
- [52] Ziesche P 1999 *Electron Correlations and Materials Properties* ed A Gonis, N Kiouassis, and M Ciftan (Kluwer/Plenum: New York), p.361
- [53] Ziesche P, Tao J, Seidl M, and Perdew J P 2000 *Int. J. Quantum Chem.* **77** 819
- [54] Cioslowski J, Ziesche P, and Pernal K 2001 *Phys. Rev. B* **63** 205105
- [55] Cioslowski J, Ziesche P, and Pernal K 2001 *J. Chem. Phys.* **115** 8725
- [56] Fuchs K 1935 *Proc. Roy. Soc. A* **151** 585
- [57] Coldwell-Horsfall R A and Maradudin A A 1960/1963 *J. Math. Phys.* **1** 395 **4** 582
- [58] Carr W J Jr. 1961 *Phys. Rev.* **122** 1437
- [59] Carr W J Jr., Coldwell-Horsfall R A, and Fein A E 1961 *Phys. Rev.* **124** 747
- [60] Diener G 1962 *Diploma Thesis* TH Dresden, cf. Ref. [32], p. 19
- [61] March N H and Sampanthar S 1962 *Acta Phys. Hung.* **14** 61
- [62] Rajagopal A K, Kimball J C, and Banerjee M 1978 *Phys. Rev. B* **18** 2339
- [63] Collins D M 1993 *Z. Naturforsch. A: Phys. Sci.* **48a** 68

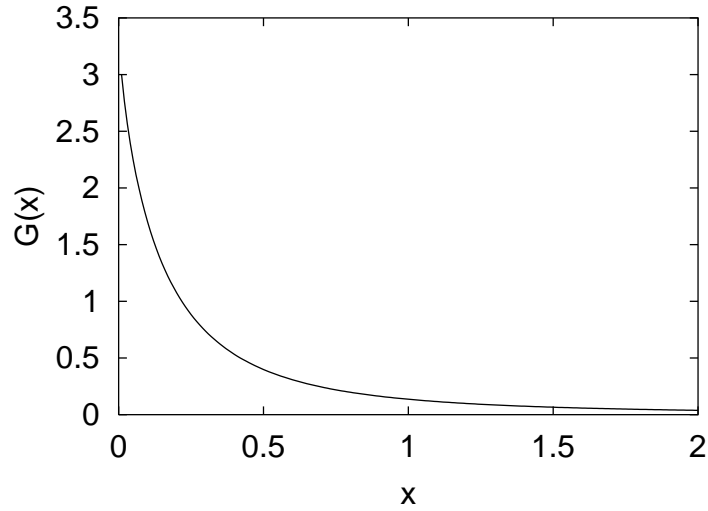


FIG. 1: The Kulik function  $G(x)$  appearing in the RPA analysis of  $n(k, r_s)$ , Eq. (A4).

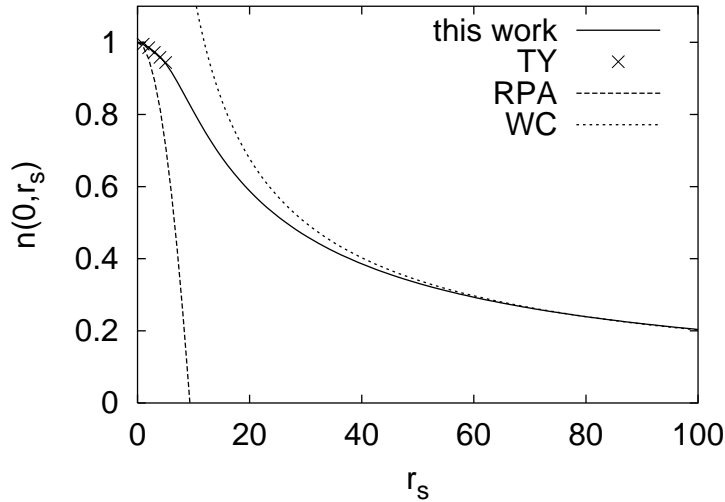


FIG. 2: Parametrized  $n(0, r_s)$  (solid line), compared to the Takada-Yasuhara (TY) values [17, 18]. The high-density or RPA limit and the Wigner crystal (WC) limit are also shown.

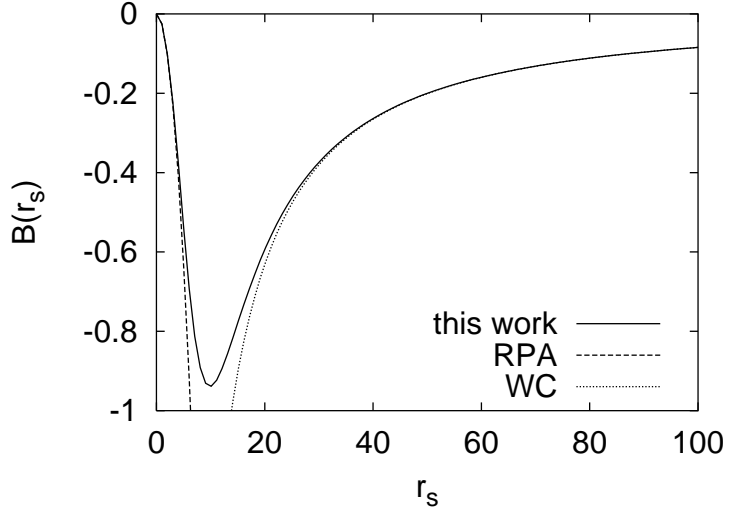


FIG. 3: Parametrized coefficient of the  $k^2$  term near the centre ( $k \rightarrow 0$ ),  $B(r_s) = -\frac{\pi^4}{\alpha^2} \frac{F''(0)}{2} \left[ \frac{r_s}{b(r_s)} \right]^2$ . The high-density or RPA result,  $b(r_s \rightarrow 0) = 1$ , and the Wigner crystal (WC) limit are also shown.

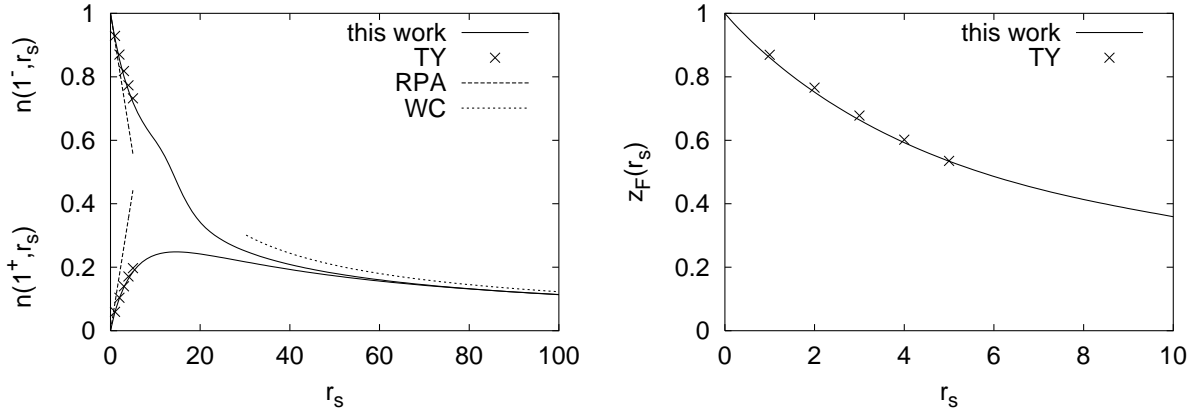


FIG. 4: Left panel: parametrized  $n(1^\pm, r_s)$  (solid lines), compared to the Takada-Yasuhara (TY) values [17, 18]. The high-density or RPA limit and the Wigner crystal (WC) limit are also shown. Right panel: value of the Fermi gap  $z_F(r_s) = n(1^-, r_s) - n(1^+, r_s)$  as a function of  $r_s$ ; the present parametrization is compared with the TY results [17, 18].

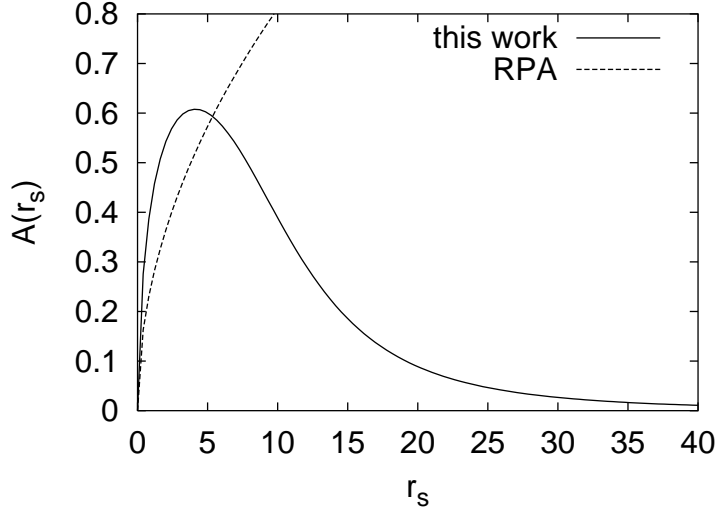


FIG. 5: Parametrized coefficient of the infinite slope at the Fermi edge,  $A(r_s) = a(r_s) \left(\frac{\alpha r_s}{\pi}\right)^{1/2} 0.63$ . The present result is compared with the RPA value,  $a(r_s \rightarrow 0) = 1$ . Note [24].

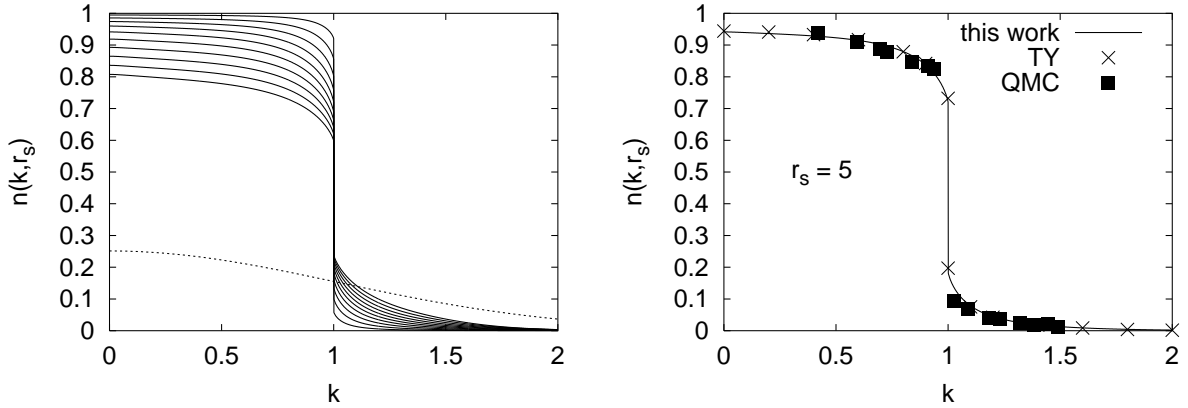


FIG. 6: Left panel: momentum distribution calculated with Eqs. (9)–(12) for  $r_s = 1, 2, \dots, 10$  (solid lines). In the Wigner limit,  $n(k, r_s \gg 1)$  is calculated with Eq. (B1) (dashed line, corresponding to  $r_s = 75$ ). Right panel: comparison of the present work with the Takada-Yasuhara (TY) [17, 18] momentum distribution and the QMC calculation of Ref. [19] for  $r_s = 5$ .

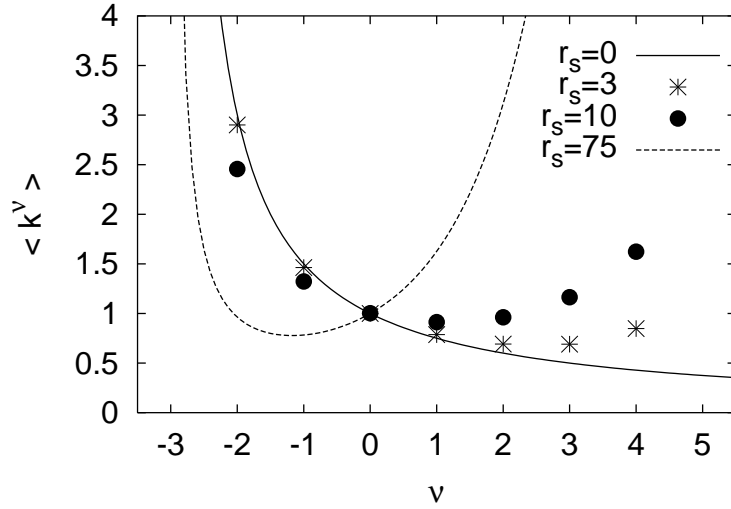


FIG. 7: The moments  $\langle k^\nu \rangle$  of  $n(k, r_s)$  for  $r_s = 3$  and  $r_s = 10$ . The corresponding results for the noninteracting gas ( $r_s = 0$ ) and for the Wigner crystal at  $r_s = 75$  are also reported.

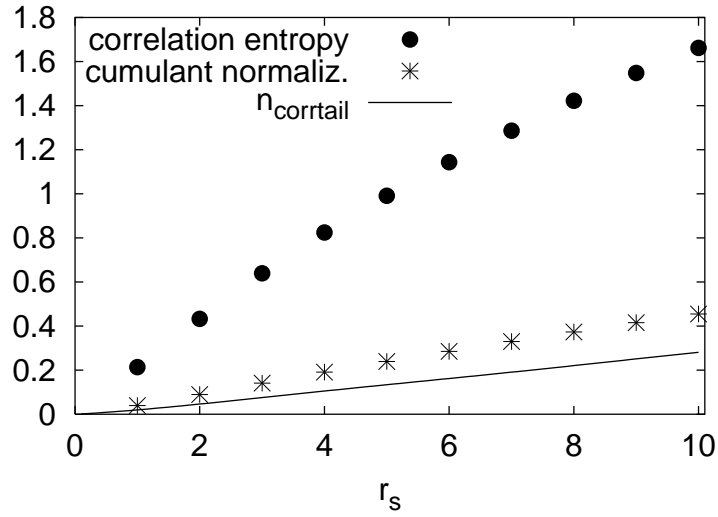


FIG. 8: The particle-hole symmetric correlation entropy [Eq. (22)], the normalization of the cumulant pair density [r.h.s. of Eq. (34)], and the correlation tail normalization  $n_{\text{corrtail}}(r_s)$  [Eq. (23)] as a function of  $r_s$ .

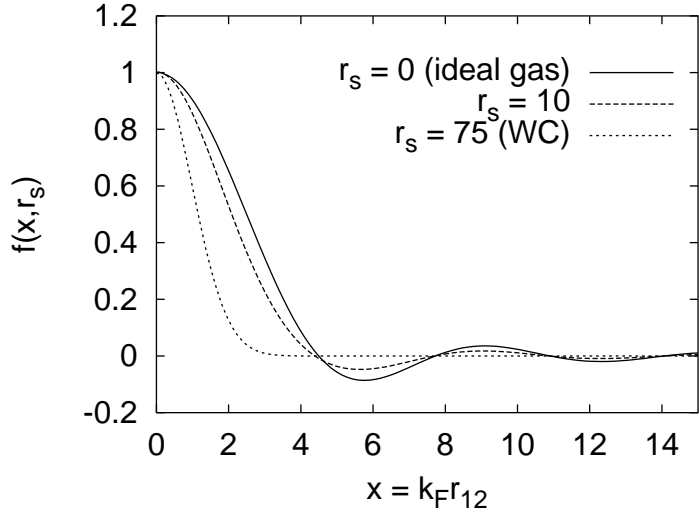


FIG. 9: 1-matrix  $f(x, r_s)$  for  $r_s = 0$  (ideal Fermi gas), for  $r_s = 10$  (present model), and for  $r_s = 75$  [Wigner crystal (WC) limit, Eq. (B1)].

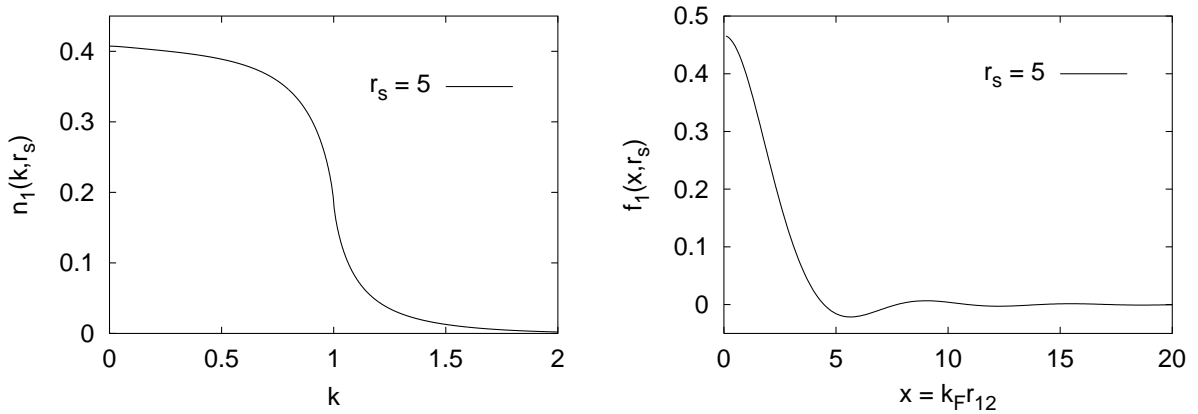


FIG. 10: Continuous part of  $n(k, r_s)$ ,  $n_1(k, r_s) = n(k, r_s) - z_F(r_s)\theta(1 - k)$  (left panel), and the corresponding 1-matrix  $f_1(x, r_s)$  (right panel). The oscillations of  $f_1(x)$  are due to the infinite slope of  $n_1(k)$  at  $k = 1$ .

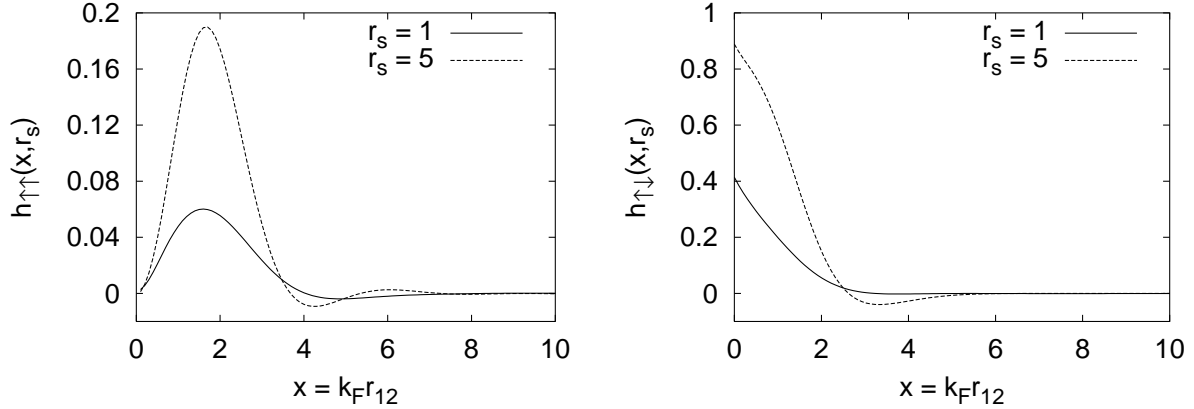


FIG. 11: Cumulant pair densities for parallel and antiparallel spins, obtained by combining the present work with the results of Ref. [27].

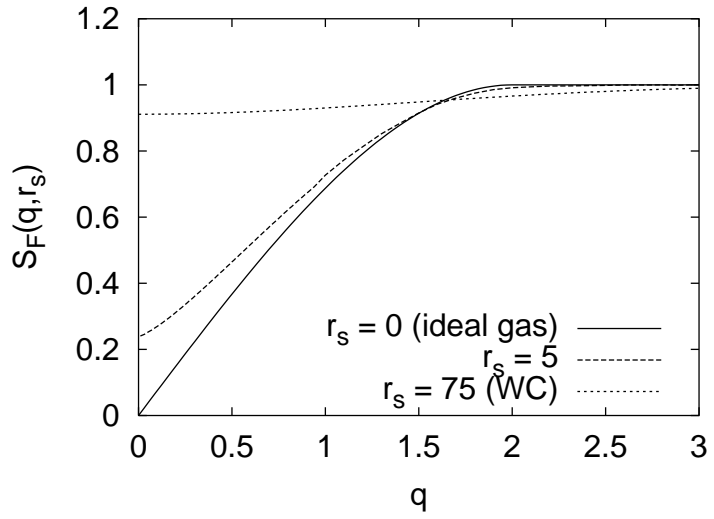


FIG. 12: The Fock component of the static structure factor for  $r_s = 0$  (ideal Fermi gas),  $r_s = 5$  (present work), and in the Wigner crystal (WC) limit for  $r_s = 75$ .

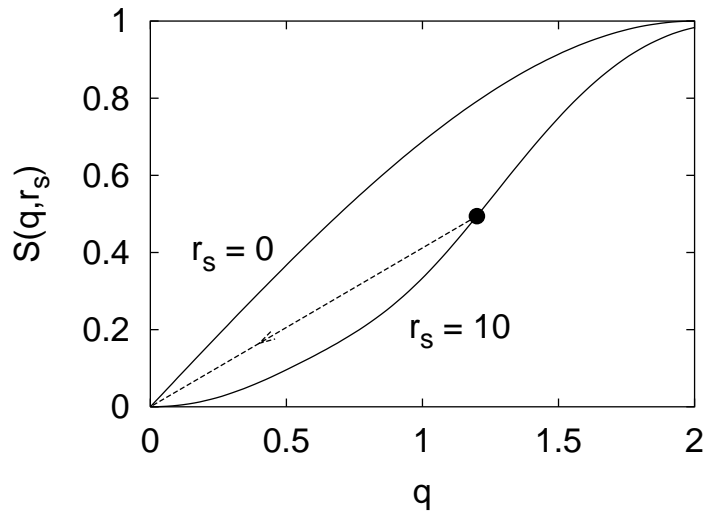


FIG. 13: Small- $q$  behavior of  $S(q, r_s)$  vs.  $q$ . The dashed line shows the trajectory of the inflexion point for  $r_s \rightarrow 0$ , schematically.